Triple-q Order in $Na_2Co_2TeO_6$ from Proximity to Hidden-SU(2)-Symmetric Point

Wilhelm G. F. Krüger,[1,*] Wenjie Chen,[2,*] Xianghong Jin,[2] Yuan Li,[2,3] and Lukas Janssen[1]
[1]Institut für Theoretische Physik and Würzburg-Dresden Cluster of Excellence ct.qmat, TU Dresden, 01062 Dresden, Germany
[2]International Center for Quantum Materials, School of Physics, Peking University, Beijing 100871, China
[3]Collaborative Innovation Center of Quantum Matter, Beijing 100871, China

(Received 12 December 2022; accepted 18 August 2023; published 5 October 2023)

In extended Heisenberg-Kitaev-Gamma-type spin models, hidden-SU(2)-symmetric points are isolated points in parameter space that can be mapped to pure Heisenberg models via nontrivial duality transformations. Such points generically feature quantum degeneracy between conventional single-**q** and exotic multi-**q** states. We argue that recent single-crystal inelastic neutron scattering data place the honeycomb magnet $Na_2Co_2TeO_6$ in proximity to such a hidden-SU(2)-symmetric point. The low-temperature order is identified as a triple-**q** state arising from the Néel antiferromagnet with staggered magnetization in the out-of-plane direction via a 4-sublattice duality transformation. This state naturally explains various distinctive features of the magnetic excitation spectrum, including its surprisingly high symmetry and the dispersive low-energy and flat high-energy bands. Our result demonstrates the importance of bond-dependent exchange interactions in cobaltates, and illustrates the intriguing magnetic behavior resulting from them.

DOI: 10.1103/PhysRevLett.131.146702

Introduction.—In the search for quantum spin liquids, the Kitaev honeycomb model [1] plays a pivotal role. It features bond-dependent exchange interactions between neighboring sites and may be realizable in magnetic Mott insulators involving heavy ions [2]. These materials are characterized by entangled spin and orbital degrees of freedom. The physical spin is no longer a good quantum number and the pseudospin degree of freedom replacing it typically features a lower symmetry that involves combined rotations in both pseudospin and lattice spaces. On the honeycomb lattice, for instance, spin-orbit coupling reduces the continuous Heisenberg SU(2) spin symmetry down to a discrete C_3^* symmetry of $2\pi/3$ pseudospin rotations about a high-symmetry axis, combined with corresponding lattice rotations [3]. This leads to a large number of symmetry-allowed exchange couplings, including Kitaev and off-diagonal Γ and Γ' interactions [4–6]. Within this large parameter space, there exist, however, isolated points that feature a *hidden* continuous SU(2) symmetry that is different from the usual Heisenberg symmetry [7,8]. These hidden-SU(2)-symmetric points can be mapped to standard Heisenberg points via duality transformations involving local pseudospin rotations [9]. The hidden SU(2) symmetry inevitably causes an SU(2) degeneracy of the model's quantum ground state. Perturbations away from such hidden-SU(2)-symmetric points can then stabilize a variety of different states, including states characterized by multiple ordering wave vectors (multi-**q** states), noncollinear pseudospin configurations, and/or large magnetic unit cells [9,10]. An interesting such state that has been studied in theoretical works of Heisenberg-Kitaev models on the honeycomb lattice is a noncollinear triple-**q** state in which each domain features three Bragg peaks in the first crystallographic Brillouin zone, with an 8-site magnetic unit cell [10,11].

Identifying such a multi-**q** state in an experiment, however, is a challenging task. The structure of the duality transformation limits the position of the Bragg peaks to a fixed set of symmetry-related points in the Brillouin zone. The Bragg-peak pattern of a single magnetic domain of a multi-**q** state, as measurable, for instance, in neutron diffraction experiments, is therefore identical to the averaged pattern of multiple domains of a corresponding single-**q** state. Since domain mixing effects are difficult to exclude in most experimental setups, the diffraction pattern of a multi-**q** state can be easily misinterpreted as a domain-averaged single-**q** pattern. A class of materials exemplifying this difficulty are d^7 honeycomb cobaltates, such as $Na_2Co_2TeO_6$, $Na_3Co_2SbO_6$, or $BaCo_2(AsO_4)_2$. These compounds have received significant interest recently as possible realizations of the Kitaev honeycomb model [12–32]. All three mentioned examples exhibit long-range magnetic order at low temperatures. Despite various experimental efforts, however, the natures of the magnetic ground states have remained under debate. In $Na_2Co_2TeO_6$, for instance, many experimental observations resemble those of α-$RuCl_3$ [3,33], which has led to the assumption that the ground state features the same zigzag type of single-**q** order [34,35]. Recent inelastic neutron scattering results on high-quality single crystals, however, have revealed a single lowest-energy magnon branch without any sign of domain superposition [19], and at least five additional nonoverlapping spin-wave branches at higher

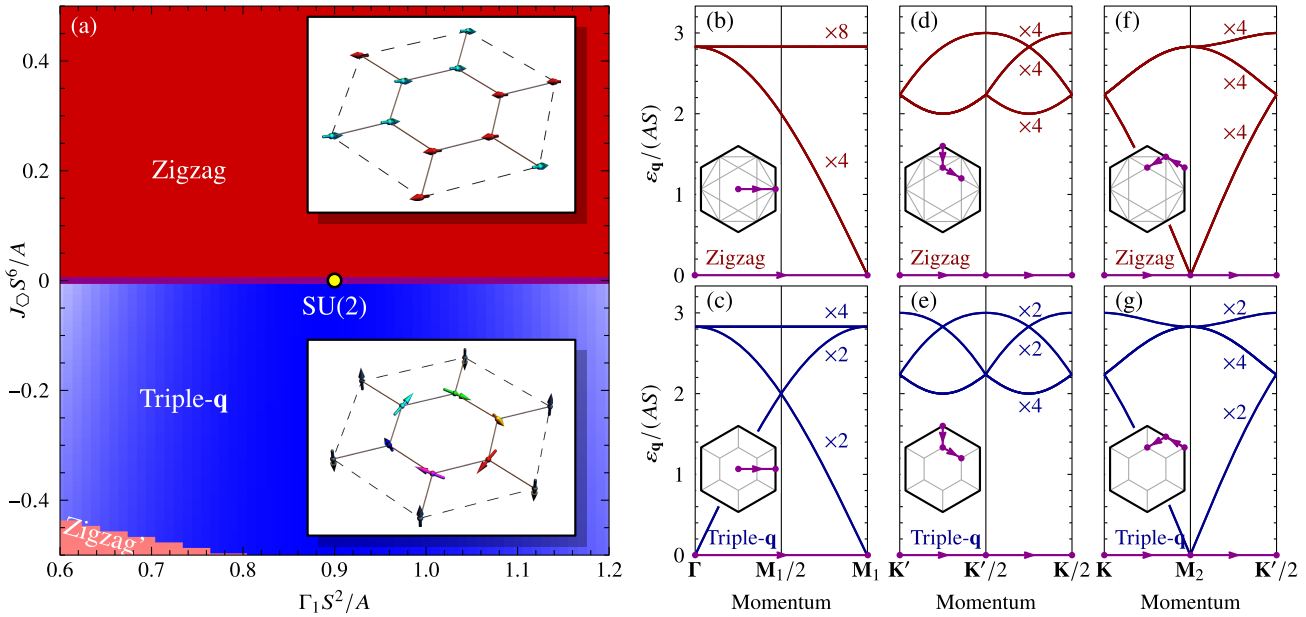

FIG. 1. (a) Classical phase diagram of HKΓΓ′ model in vicinity of hidden-SU(2)-symmetric point (yellow dot) in the plane spanned by off-diagonal coupling Γ_1 and ring exchange coupling $J_\bigcirc$, from classical Monte Carlo simulations. For $J_\bigcirc > 0$ ($J_\bigcirc < 0$), zigzag (triple-**q**) order with a 4-site (8-site) magnetic unit cell is stabilized, see insets. Color scales indicate Bragg-peak intensities in different phases in arbitrary units. The zigzag' phase at small Γ_1 and large negative $J_\bigcirc$ is characterized by a 4-site unit cell, in which the spins along zigzag chains become slightly noncollinear. (b)–(g) Magnon dispersions from linear spin-wave theory at hidden-SU(2)-symmetric point for (b), (d),(f) domain-averaged zigzag order and (c),(e),(g) triple-**q** order, along different trajectories within the first structural Brillouin zone, as displayed in insets. The triple-**q** spectra are symmetric along these trajectories, while the zigzag spectra are not. This can be understood as a consequence of the difference in shape and size of the magnetic Brillouin zones, indicated in gray in the insets.

energy [27], which may be indicative of a multi-**q** state. Furthermore, nuclear magnetic resonance experiments have suggested a noncollinear magnetic structure that is inconsistent with the simple zigzag ordering [20]. These results are at odds with all spin models proposed for $Na_2Co_2TeO_6$ to date, all of which feature a zigzag ground state [17,18,23,25]. A similar ambiguity between single-**q** and multi-**q** scenarios arises for $Na_3Co_2SbO_6$ [28] on the honeycomb lattice, as well as for $Co_{1/3}TaS_2$ on the triangular lattice [36].

In this Letter, we demonstrate how a multi-**q** state that features Bragg peaks at symmetry-related points in the crystallographic Brillouin zone can be uniquely identified. We exploit the fact that the *shape* of the magnetic Brillouin zone in a multi-**q** state differs from those of the corresponding single-**q** states. This leads to different symmetries of the magnetic excitation energies. Applying this approach to $Na_2Co_2TeO_6$, for which high-resolution spectra are available [27], reveals a noncollinear triple-**q** ground state with a hexagonally shaped magnetic unit cell featuring 8 magnetic sites. An effective model, which features nonbilinear exchange interactions in addition to the usual Heisenberg-Kitaev-Gamma-type exchanges, stabilizes the triple-**q** order and reproduces important features in the measured magnetic excitation spectrum very well.

Model.—To understand the novel physics of the d^7 honeycomb cobaltates, consider an extended Heisenberg-Kitaev-Gamma-Gamma′ (HKΓΓ′) model,

$$\mathcal{H} = \sum_{\gamma=x,y,z} \sum_{\langle ij\rangle_\gamma} \Big[J_1 \mathbf{S}_i \cdot \mathbf{S}_j + K_1 S_i^\gamma S_j^\gamma + \Gamma_1 (S_i^\alpha S_j^\beta + S_i^\beta S_j^\alpha) + \Gamma_1' (S_i^\gamma S_j^\alpha + S_i^\alpha S_j^\gamma + S_i^\gamma S_j^\beta + S_i^\beta S_j^\gamma) \Big] + \sum_{\langle\langle\langle ij\rangle\rangle\rangle} J_3 \mathbf{S}_i \cdot \mathbf{S}_j + \sum_{\langle\langle ij\rangle\rangle^A} J_2^A \mathbf{S}_i \cdot \mathbf{S}_j + \sum_{\langle\langle ij\rangle\rangle^B} J_2^B \mathbf{S}_i \cdot \mathbf{S}_j + \mathcal{H}_{\text{nbl}}, \quad (1)$$

where $\langle ij\rangle_\gamma$ denotes first-neighbor γ bonds on the honeycomb lattice, and $\langle\langle\langle ij\rangle\rangle\rangle$ are third-neighbor bonds along opposite sites of the same hexagon. J_1 and J_3 are the corresponding first- and third-neighbor Heisenberg couplings, K_1 the first-neighbor Kitaev coupling, and Γ_1 and Γ_1' the two first-neighbor symmetric off-diagonal couplings. $\langle\langle ij\rangle\rangle^A$ and $\langle\langle ij\rangle\rangle^B$ correspond to second-neighbor bonds between sites on the same sublattice A and B, respectively. Here, we have taken a possible sublattice symmetry breaking into account, parametrized by the two second-neighbor Heisenberg couplings J_2^A and J_2^B. In $Na_2Co_2TeO_6$, sublattice symmetry breaking arises from the two crystallographically inequivalent Co^{2+} sites [16]. Finally, $\mathcal{H}_{\text{nbl}}$ denotes nonbilinear exchange interactions, such as ring exchanges. These can be understood as leading corrections to the first-neighbor bilinear exchange in the strong-coupling expansion of the Hubbard model [37–40], and are important in a number of $3d$

materials, including various chromium-, manganese-, and copper-based magnets [41–44]. They will be specified below.

Hidden SU(2) symmetries.—For particular values of the exchange couplings, the HKΓΓ′ model defined above features hidden SU(2) symmetries that can be revealed via suitable duality transformations [9]. These transformations correspond to local spin rotations and map the hidden-SU(2)-symmetric HKΓΓ′ model for the original spins to a pure Heisenberg model for the dual spins. In the parameter regime $K_1 < 0$, relevant for the cobaltates [12,13], such a hidden-SU(2)-symmetric point can be identified by a $\mathcal{T}_1\mathcal{T}_4$ transformation. Here, $\mathcal{T}_1$ corresponds to a global π rotation about the [111] axis in cubic spin space, whereas $\mathcal{T}_4$ denotes the 4-sublattice transformation that corresponds to a π rotation about the x, y, and z axes at sublattices 1, 2, and 3, respectively, and no rotation at sublattice 4 [45], Sec. (a). Inverting the transformation maps the HKΓΓ′ model with $\mathcal{H}_{\mathrm{nbl}} = 0$ and bilinear couplings

$$(J_1, K_1, \Gamma_1, \Gamma_1', J_2^A, J_2^B)_{\mathrm{SU}(2)} = \left(-\frac{1}{9}, -\frac{2}{3}, \frac{8}{9}, -\frac{4}{9}, 0, 0\right) A, \quad (2)$$

and arbitrary J_3, where $A > 0$ corresponds to the overall energy scale, to a $\tilde{J}_1$-$\tilde{J}_3$ Heisenberg model for the dual spins, with dual couplings $\tilde{J}_1 = A$ and $\tilde{J}_3 = J_3$. At this hidden-SU(2)-symmetric point, the HKΓΓ′ model features an SU(2)-degenerate ground-state manifold, each member of which can be mapped to an associated ground state of the dual $\tilde{J}_1$-$\tilde{J}_3$ model, and vice versa. The Néel state in the dual model with staggered magnetization along the x, y, and z cubic axes, for instance, maps to the zigzag state in the original model with antiferromagnetic neighbor pairs along the x, y, and z bonds, respectively, see upper inset of Fig. 1(a). The Néel state with staggered magnetization along the [111] axis, by contrast, maps to a triple-**q** state with an 8-site magnetic unit cell and a vortex spin structure on 1/4 of the hexagonal plaquettes, see lower inset of Fig. 1(a).

While bilinear exchange perturbations cannot lift the SU(2) degeneracy in the classical limit, and quantum fluctuations typically favor collinear zigzag states [45], Sec. (b), a triple-**q** state can be stabilized by nonbilinear exchange interactions. To be specific, let us consider the ring exchange that is generated in the strong-coupling expansion of the single-band $t-U$ Hubbard model on the honeycomb lattice [40],

$$\begin{aligned} H_{\mathrm{nbl}} &= \frac{J_\bigcirc}{6} \sum_{\langle ijklmn \rangle} [2(\mathbf{S}_i \cdot \mathbf{S}_j)(\mathbf{S}_k \cdot \mathbf{S}_l)(\mathbf{S}_m \cdot \mathbf{S}_n) \\ &\quad - 6(\mathbf{S}_i \cdot \mathbf{S}_k)(\mathbf{S}_j \cdot \mathbf{S}_l)(\mathbf{S}_m \cdot \mathbf{S}_n) + 3(\mathbf{S}_i \cdot \mathbf{S}_l)(\mathbf{S}_j \cdot \mathbf{S}_k)(\mathbf{S}_m \cdot \mathbf{S}_n) \\ &\quad + 3(\mathbf{S}_i \cdot \mathbf{S}_k)(\mathbf{S}_j \cdot \mathbf{S}_m)(\mathbf{S}_l \cdot \mathbf{S}_n) - (\mathbf{S}_i \cdot \mathbf{S}_l)(\mathbf{S}_j \cdot \mathbf{S}_m)(\mathbf{S}_k \cdot \mathbf{S}_n) \\ &\quad + \text{cyclic permutations of } (ijklmn)], \end{aligned} \quad (3)$$

with summation over elemental plaquettes involving sites $(ijklmn)$ in counterclockwise order. In $Na_2Co_2TeO_6$, the above nonbilinear interaction arises from virtual ring exchange processes of cobalt electrons around elemental plaquettes on the honeycomb lattice, with the prefactors originating from the number of symmetry-equivalent processes and the involved permutations [53]. Formally, this form of the interaction is generated at sixth order in the strong-coupling expansion. At intermediate coupling, however, it represents the main correction to the

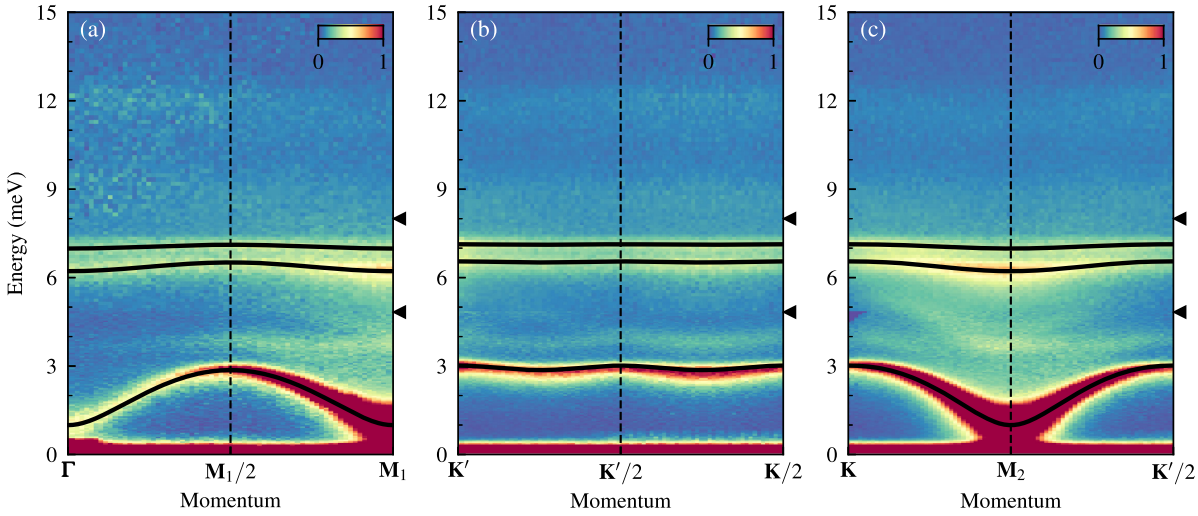

FIG. 2. Inelastic neutron scattering intensity of $Na_2Co_2TeO_6$ at $T = 5$ K along momentum trajectories indicated in insets of Figs. 1(b)–1(g). Data are measured with $E_i = 19.4$ meV (upper part), $E_i = 10.0$ meV (middle part), $E_i = 6.1$ meV (lower part), and merged at energies indicated by left-pointing triangles. All visible magnon bands are symmetric along these trajectories, indicating a hexagonal magnetic Brillouin zone with an 8-site real-space magnetic unit cell. Black solid lines indicate three representative magnon band dispersions parametrized with phenomenological functions [45], Sec. (d), which are our fitting targets.

nearest-neighbor exchange J_1, exceeding the second-neighbor exchange J_2, which formally arises already at fourth order in the expansion: For instance, at $t/U = 0.2$, Ref. [40] finds $|J_\bigcirc/J_2| \simeq 4$. Near the hidden-SU(2)-symmetric point, this ring exchange favors triple-**q** order for $J_\bigcirc < 0$, see Fig. 1(a). For the cobaltates, various different nonbilinear exchange terms are in principle possible, and the ring coupling $J_\bigcirc$ defined above constitutes only one representative axis in a large parameter space. For symmetry reasons, however, all of these couplings will generically have the same qualitative effect: They will favor zigzag order on one side of the hidden-SU(2)-symmetric point and triple-**q** order on the other side.

Magnetic excitation spectrum.—Each zigzag domain has a rectangular magnetic Brillouin zone. The triple-**q** state, by contrast, features a hexagonal Brillouin zone. The difference in the shape of the magnetic Brillouin zones leads to decisive consequence for the magnetic excitation spectrum. To illustrate this, let us consider the hidden-SU(2)-symmetric point. Figures 1(b)–1(g) compare the magnon spectrum in the zigzag state (top row) with those of the triple-**q** state (bottom row), for three different paths within the first crystallographic Brillouin zone, in linear spin-wave theory. These paths cover points that are related by the symmetry of the triple-**q** state, but not of the zigzag state. This allows the identification of triple-**q** order: While the triple-**q** magnon spectrum is symmetric with respect to these paths, the zigzag spectrum is not. We emphasize that this symmetry argument is independent of a particular modeling, and applies equally to excitation beyond linear spin-wave theory, such as magnon bound states or lower bounds of magnetic excitation continua. It does not apply, however, to scattering intensities, which depend on absolute momenta.

Figure 2 shows the low-temperature neutron scattering intensity of $Na_2Co_2TeO_6$ along the same paths as in Figs. 1(b)–1(g), compiled from the experimental data initially published in Ref. [27]. Remarkably, all visible magnon bands are perfectly symmetric along these trajectories, clearly indicating a hexagonal magnetic Brillouin zone with an 8-site real-space unit cell. Moreover, several qualitative features of the measured spectrum can be understood from the triple-**q** spectrum at the hidden-SU(2)-symmetric point. This includes the dispersive low-energy and flat high-energy bands, the number of excitation energies at the **Γ** point, as well as the small gap $\sim$1 meV at both **Γ** and **M**. The latter can be considered as a pseudo-Goldstone mode arising from the explicit breaking of the hidden-SU(2) symmetry, and be a measure of proximity to the hidden-SU(2)-symmetric point.

Effective model for $Na_2Co_2TeO_6$.—The above comparison suggests that the magnetic excitation spectrum in the low-temperature ordered phase of $Na_2Co_2TeO_6$ can be modeled using a parameter set proximate to the hidden-SU(2)-symmetric point. In linear-spin-wave theory, the ring exchange can be mapped to an effective local field along the local-moment axis, together with a renormalization of the bilinear couplings [45], Sec. (c). In order to simplify the fitting algorithm, and to avoid the ambiguity arising from the various symmetry-allowed nonbilinear terms, we here constrain ourselves to an effective modeling using the local-field term directly, mimicking a ring exchange, i.e., $\mathcal{H}_{\mathrm{nbl}} \simeq -h \sum_i \mathbf{n}_i \cdot \mathbf{S}_i$, with unit vector $\mathbf{n}_i$ along the triple-**q** spin direction at the hidden-SU(2)-symmetric point. An alternative fitting procedure using the full ring exchange of Eq. (3) leads to similar results [45], Sec. (d). Optimizing the parameters with respect to the three spin-wave modes indicated by black lines in Fig. 2 [see Ref. [45], Sec. (d) for details] leads to our best-fit model,

$$(J_1, K_1, \Gamma_1, \Gamma_1', J_2^A, J_2^B, J_3)_{\mathrm{fit}} = (1.23, -8.29, 1.86, -2.27, 0.32, -0.24, 0.47)\ \mathrm{meV}, \quad (4)$$

and $h = 0.88$ meV, for $S = 1/2$. The resulting magnetic excitation spectrum is shown in Fig. 3, to be compared with Fig. 3(a) of Ref. [27]. Importantly, the computed spectrum does not only reflect favorably the three fitting targets

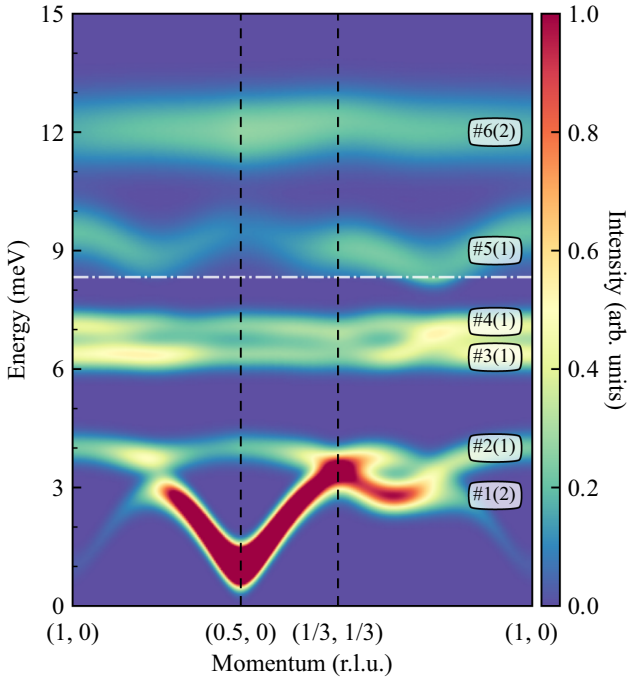

FIG. 3. Magnetic excitation spectrum from linear spin-wave theory of best-fit model, Eq. (4), to be compared with Fig. 3(a) of Ref. [27]. The ground state is optimized to acquire the lowest energy, realizing the triple-**q** order shown in the lower inset of Fig. 1(a). Different full width at half maxima (FWHM) are used in simulations at higher and lower energies for better comparison with experimental data: FWHM($E > 8.3$ meV) = 1.18 meV, FWHM($E < 8.3$ meV) = 0.59 meV. Branch indices are indicated after [27], along with their practical degeneracy (defined as the number of branches within the FWHM).

(modes No. 1, No. 3, and No. 4), but moreover reproduces remarkably well also the other experimentally observed modes No. 2, No. 5, and No. 6, both in terms of their bandwidths as well as their absolute energies. Further comparisons between theoretical and experimental results, as well as a juxtaposition with results of a best-fit model with zigzag ground state, are presented in [45], Sec. (e).

Discussion.—Our best-fit model suggests that the most dominant bilinear perturbation away from the hidden-SU(2)-symmetric point is towards the ferromagnet Kitaev limit. In [45], Sec. (f), we present extensive exact diagonalization calculations that show that $Na_2Co_2TeO_6$ is in fact similarly close to the Kitaev quantum spin liquid regime as other intensely studied Kitaev candidate materials, including Na_2IrO_3 and α-$RuCl_3$. Hence, while the low-temperature behavior in the triple-**q** phase can be well understood within the picture of approximate hidden-SU(2) symmetry, the nearby Kitaev quantum spin liquid should be expected to play an essential role at intermediate temperature and in external magnetic fields, when the magnetic order is melted [16,18–21,26]. In fact, the effective energy scale set by the Kitaev coupling of our best-fit model $|K_1|/k_B \simeq 8.3$ meV$/k_B \sim 100$ K is well above the Néel temperature $T_N \simeq 30$ K [19,27,35], leaving an intermediate temperature regime that might be best described as a Kitaev paramagnet, similar to what has been observed in α-$RuCl_3$ [54–57]. Furthermore, the noncollinear zero-field ordering implies increased magnetic frustration in external fields, as not all spins can cant homogeneously towards the field axis [58,59]. As a consequence, a spin model proximate to the hidden-SU(2)-symmetric point generically features a metamagnetic transition between the triple-**q** state at small fields and a canted zigzag state at intermediate fields, before the transition towards the paramagnetic state at high fields, see Ref. [45], Sec. (g) for details. A recent variational Monte Carlo study also suggests a possible field-induced transition from a triple-**q** state at small fields towards a field-induced quantum spin liquid at intermediate in-plane fields [46]. We expect these features of our minimal models to explain at least some of the various thermal and field-induced transitions observed in $Na_2Co_2TeO_6$ [19–21,60,61].

Conclusions.—We have demonstrated how a multi-**q** state that features Bragg peaks at symmetry-related points in the Brillouin zone can be distinguished experimentally from the corresponding multidomain single-**q** state. While the Bragg-peak pattern of both states can be identical, the difference in shape of the magnetic Brillouin zones leads to different symmetries of the magnetic excitation spectra. Applying this approach to the honeycomb magnet $Na_2Co_2TeO_6$ allows the identification of the material's low-temperature magnetic order: a triple-**q** state with a hexagonal 8-site magnetic unit cell and a vortex spin structure around 1/4 of the elemental plaquettes. Our result reveals $Na_2Co_2TeO_6$ as an example of a Kitaev magnet proximate to a hidden-SU(2)-symmetric point. This explains not only the small band gap of the pseudo-Goldstone mode, but also the dispersive low-energy and flat high-energy bands observed in the spectrum. The most dominant perturbation away from the hidden-SU(2)-symmetric point, however, is towards the ferromagnet Kitaev limit, and plays an essential role at intermediate temperature and in external magnetic fields. This represents an intriguing question for future research. In a broader context, our results suggest that the symmetry of the magnetic excitation spectrum may be worth reanalyzing also in other Kitaev magnets, such as $Na_3Co_2SbO_6$ [28], or again α-$RuCl_3$ [56,59,62–65]. The latter displays multiple uniform Bragg peaks in fields below 1–2 T [64,66], a fact that was previously interpreted in terms of domain mixing arising from bond anisotropies [67,68], but could, in principle, also stem from multi-**q** order.

Note added.—A parallel work reports in-field neutron diffraction data of $Na_2Co_2TeO_6$, which are consistent with our results [72].

We thank Fakher Assaad, Bernd Büchner, Jeroen van den Brink, Matthias Gillig, Christian Hess, Xiaochen Hong, Vladik Kataev, Vilmos Kocsis, Zheng-Xin Liu, Satoshi Nishimoto, Matthias Vojta, Jiucai Wang, Christoph Wellm, and Anja Wolter for illuminating discussions and collaboration on related work. We are grateful to Weiliang Yao for assistance on extracting some of the neutron scattering data originally published in [27]. The data were obtained with the support of Kazuki Iida and Kazuya Kamazawa at the MLF, J-PARC, Japan, under a user program (Proposal No. 2019B0062). Spin-wave calculations involved in the fitting procedure were performed on a computing cluster at Peking University using SpinW [69]. Exact diagonalization calculations were performed on a computing cluster at TU Dresden using QuSpin [70,71]. The work of W. G. F. K. and L. J. is supported by the Deutsche Forschungsgemeinschaft (DFG) through SFB 1143 (A07, Project No. 247310070), the Würzburg-Dresden Cluster of Excellence *ct.qmat* (EXC 2147, Project No. 390858490), and the Emmy Noether program (JA2306/4-1, Project No. 411750675). The work of W. C., X. J., and Y. L. is partly supported by the National Natural Science Foundation of China (NSFC, Grant No. 12061131004).

[*] These two authors contributed equally to this work.

[1] A. Kitaev, Anyons in an exactly solved model and beyond, Ann. Phys. (N.Y.) **321**, 2 (2006).
[2] S. Trebst and C. Hickey, Kitaev materials, Phys. Rep. **950**, 1 (2022).
[3] L. Janssen and M. Vojta, Heisenberg-Kitaev physics in magnetic fields, J. Phys. Condens. Matter **31**, 423002 (2019).

[4] J. Chaloupka, G. Jackeli, and G. Khaliullin, Zigzag Magnetic Order in the Iridium Oxide Na_2IrO_3, Phys. Rev. Lett. **110**, 097204 (2013).

[5] J. G. Rau, Eric Kin-Ho Lee, and H.-Y. Kee, Generic Spin Model for the Honeycomb Iridates beyond the Kitaev Limit, Phys. Rev. Lett. **112**, 077204 (2014).

[6] S. M. Winter, A. A. Tsirlin, M. Daghofer, J. van den Brink, Y. Singh, P. Gegenwart, and R. Valentí, Models and materials for generalized Kitaev magnetism, J. Phys. Condens. Matter **29**, 493002 (2017).

[7] J. Chaloupka, G. Jackeli, and G. Khaliullin, Kitaev-Heisenberg Model on a Honeycomb Lattice: Possible Exotic Phases in Iridium Oxides A_2IrO_3, Phys. Rev. Lett. **105**, 027204 (2010).

[8] I. Kimchi and A. Vishwanath, Kitaev-Heisenberg models for iridates on the triangular, hyperkagome, kagome, fcc, and pyrochlore lattices, Phys. Rev. B **89**, 014414 (2014).

[9] J. Chaloupka and G. Khaliullin, Hidden symmetries of the extended Kitaev-Heisenberg model: Implications for the honeycomb-lattice iridates A_2IrO_3, Phys. Rev. B **92**, 024413 (2015).

[10] L. Janssen, E. C. Andrade, and M. Vojta, Honeycomb-Lattice Heisenberg-Kitaev Model in a Magnetic Field: Spin Canting, Metamagnetism, and Vortex Crystals, Phys. Rev. Lett. **117**, 277202 (2016).

[11] P. M. Cônsoli, L. Janssen, M. Vojta, and E. C. Andrade, Heisenberg-Kitaev model in a magnetic field: $1/S$ expansion, Phys. Rev. B **102**, 155134 (2020).

[12] H. Liu and G. Khaliullin, Pseudospin exchange interactions in d^7 cobalt compounds: Possible realization of the Kitaev model, Phys. Rev. B **97**, 014407 (2018).

[13] R. Sano, Y. Kato, and Y. Motome, Kitaev-Heisenberg Hamiltonian for high-spin d^7 Mott insulators, Phys. Rev. B **97**, 014408 (2018).

[14] J.-Q. Yan, S. Okamoto, Y. Wu, Q. Zheng, H. D. Zhou, H. B. Cao, and M. A. McGuire, Magnetic order in single crystals of $Na_3Co_2SbO_6$ with a honeycomb arrangement of $3d^7$ Co^{2+} ions, Phys. Rev. Mater. **3**, 074405 (2019).

[15] H. Liu, J. Chaloupka, and G. Khaliullin, Kitaev Spin Liquid in $3d$ Transition Metal Compounds, Phys. Rev. Lett. **125**, 047201 (2020).

[16] W. Yao and Y. Li, Ferrimagnetism and anisotropic phase tunability by magnetic fields in $Na_2Co_2TeO_6$, Phys. Rev. B **101**, 085120 (2020).

[17] M. Songvilay, J. Robert, S. Petit, J. A. Rodriguez-Rivera, W. D. Ratcliff, F. Damay, V. Balédent, M. Jiménez-Ruiz, P. Lejay, E. Pachoud, A. Hadj-Azzem, V. Simonet, and C. Stock, Kitaev interactions in the Co honeycomb antiferromagnets $Na_3Co_2SbO_6$ and $Na_2Co_2TeO_6$, Phys. Rev. B **102**, 224429 (2020).

[18] G. Lin *et al.*, Field-induced quantum spin disordered state in spin-1/2 honeycomb magnet $Na_2Co_2TeO_6$, Nat. Commun. **12**, 5559 (2021).

[19] W. Chen, X. Li, Z. Hu, Z. Hu, L. Yue, R. Sutarto, F. He, K. Iida, K. Kamazawa, W. Yu, X. Lin, and Y. Li, Spin-orbit phase behavior of $Na_2Co_2TeO_6$ at low temperatures, Phys. Rev. B **103**, L180404 (2021).

[20] C. H. Lee, S. Lee, Y. S. Choi, Z. H. Jang, R. Kalaivanan, R. Sankar, and K.-Y. Choi, Multistage development of anisotropic magnetic correlations in the Co-based honeycomb lattice $Na_2Co_2TeO_6$, Phys. Rev. B **103**, 214447 (2021).

[21] X. Hong, M. Gillig, R. Hentrich, W. Yao, V. Kocsis, A. R. Witte, T. Schreiner, D. Baumann, N. Pérez, A. U. B. Wolter, Y. Li, B. Büchner, and C. Hess, Strongly scattered phonon heat transport of the candidate Kitaev material $Na_2Co_2TeO_6$, Phys. Rev. B **104**, 144426 (2021).

[22] A. M. Samarakoon, Q. Chen, H. Zhou, and V. O. Garlea, Static and dynamic magnetic properties of honeycomb lattice antiferromagnets $Na_2M_2TeO_6$, $M = \mathrm{Co}$ and Ni, Phys. Rev. B **104**, 184415 (2021).

[23] C. Kim, J. Jeong, G. Lin, P. Park, T. Masuda, S. Asai, S. Itoh, H.-S. Kim, H. Zhou, J. Ma, and J.-G. Park, Antiferromagnetic Kitaev interaction in $J_{\mathrm{eff}} = 1/2$ cobalt honeycomb materials $Na_3Co_2SbO_6$ and $Na_2Co_2TeO_6$, J. Phys. Condens. Matter **34**, 045802 (2022).

[24] S. Mukherjee, G. Manna, P. Saha, S. Majumdar, and S. Giri, Ferroelectric order with a linear high-field magnetoelectric coupling in $Na_2Co_2TeO_6$: A proposed Kitaev compound, Phys. Rev. Mater. **6**, 054407 (2022).

[25] A. L. Sanders, R. A. Mole, J. Liu, A. J. Brown, D. Yu, C. D. Ling, and S. Rachel, Dominant Kitaev interactions in the honeycomb materials $Na_3Co_2SbO_6$ and $Na_2Co_2TeO_6$, Phys. Rev. B **106**, 014413 (2022).

[26] H. Yang, C. Kim, Y. Choi, J. H. Lee, G. Lin, J. Ma, M. Kratochvílová, P. Proschek, E.-G. Moon, K. H. Lee, Y. S. Oh, and J.-G. Park, Significant thermal Hall effect in the $3d$ cobalt Kitaev system $Na_2Co_2TeO_6$, Phys. Rev. B **106**, L081116 (2022).

[27] W. Yao, K. Iida, K. Kamazawa, and Y. Li, Excitations in the Ordered and Paramagnetic States of Honeycomb Magnet $Na_2Co_2TeO_6$, Phys. Rev. Lett. **129**, 147202 (2022).

[28] X. Li, Y. Gu, Y. Chen, V. O. Garlea, K. Iida, K. Kamazawa, Y. Li, G. Deng, Q. Xiao, X. Zheng, Z. Ye, Y. Peng, I. A. Zaliznyak, J. M. Tranquada, and Y. Li, Giant Magnetic In-Plane Anisotropy and Competing Instabilities in $Na_3Co_2SbO_6$, Phys. Rev. X **12**, 041024 (2022).

[29] R. Zhong, T. Gao, N. P. Ong, and R. J. Cava, Weak-field induced nonmagnetic state in a Co-based honeycomb, Sci. Adv. **6**, eaay6953 (2020).

[30] L. Y. Shi, X. M. Wang, R. D. Zhong, Z. X. Wang, T. C. Hu, S. J. Zhang, Q. M. Liu, T. Dong, F. Wang, and N. L. Wang, Magnetic excitations of the field-induced states in $BaCo_2(AsO_4)_2$ probed by time-domain terahertz spectroscopy, Phys. Rev. B **104**, 144408 (2021).

[31] X. Zhang, Y. Xu, T. Halloran, R. Zhong, C. Broholm, R. J. Cava, N. Drichko, and N. P. Armitage, A magnetic continuum in the cobalt-based honeycomb magnet $BaCo_2(AsO_4)_2$, Nat. Mater. **22**, 58 (2023).

[32] S. M. Winter, Magnetic couplings in edge-sharing high-spin d^7 compounds, JPhys Mater. **5**, 045003 (2022).

[33] H. Takagi, T. Takayama, G. Jackeli, G. Khaliullin, and S. E. Nagler, Concept and realization of Kitaev quantum spin liquids, Nat. Rev. Phys. **1**, 264 (2019).

[34] E. Lefrançois, M. Songvilay, J. Robert, G. Nataf, E. Jordan, L. Chaix, C. V. Colin, P. Lejay, A. Hadj-Azzem, R. Ballou, and V. Simonet, Magnetic properties of the honeycomb oxide $Na_2Co_2TeO_6$, Phys. Rev. B **94**, 214416 (2016).

[35] A. K. Bera, S. M. Yusuf, A. Kumar, and C. Ritter, Zigzag antiferromagnetic ground state with anisotropic correlation lengths in the quasi-two-dimensional honeycomb lattice compound $Na_2Co_2TeO_6$, Phys. Rev. B **95**, 094424 (2017).

[36] P. Park, W. Cho, C. Kim, Y. An, Y.-G. Kang, M. Avdeev, R. Sibille, K. Iida, R. Kajimoto, K. H. Lee, W. Ju, E.-J. Cho, H.-J. Noh, M. J. Han, S.-S. Zhang, C. D. Batista, and J.-G. Park, Tetrahedral triple-Q ordering in the metallic triangular lattice antiferromagnet $Co_{1/3}TaS_2$, arXiv:2303.03760.

[37] M. Takahashi, Half-filled Hubbard model at low temperature, J. Phys. C **10**, 1289 (1977).

[38] A. H. MacDonald, S. M. Girvin, and D. Yoshioka, t/U expansion for the Hubbard model, Phys. Rev. B **37**, 9753 (1988).

[39] H.-Y. Yang, A. M. Läuchli, F. Mila, and K. P. Schmidt, Effective Spin Model for the Spin-Liquid Phase of the Hubbard Model on the Triangular Lattice, Phys. Rev. Lett. **105**, 267204 (2010).

[40] H.-Y. Yang, A. F. Albuquerque, S. Capponi, A. M. Läuchli, and K. P. Schmidt, Effective spin couplings in the Mott insulator of the honeycomb lattice Hubbard model, New J. Phys. **14**, 115027 (2012).

[41] Y. O. Kvashnin, A. Bergman, A. I. Lichtenstein, and M. I. Katsnelson, Relativistic exchange interactions in CrX_3 ($X = $ Cl, Br, I) monolayers, Phys. Rev. B **102**, 115162 (2020).

[42] N. S. Fedorova, C. Ederer, N. A. Spaldin, and A. Scaramucci, Biquadratic and ring exchange interactions in orthorhombic perovskite manganites, Phys. Rev. B **91**, 165122 (2015).

[43] B. Dalla Piazza, M. Mourigal, M. Guarise, H. Berger, T. Schmitt, K. J. Zhou, M. Grioni, and H. M. Rønnow, Unified one-band Hubbard model for magnetic and electronic spectra of the parent compounds of cuprate superconductors, Phys. Rev. B **85**, 100508(R) (2012).

[44] C. B. Larsen, A. T. Rømer, S. Janas, F. Treue, B. Mønsted, N. E. Shaik, H. M. Rønnow, and K. Lefmann, Exact diagonalization study of the Hubbard-parametrized four-spin ring exchange model on a square lattice, Phys. Rev. B **99**, 054432 (2019).

[45] See Supplemental Material at http://link.aps.org/supplemental/10.1103/PhysRevLett.131.146702, which includes Refs. [46–52], for (a) details about the $\mathcal{T}_1\mathcal{T}_4$ duality transformation, (b) a discussion of perturbations away from the hidden-SU(2)-symmetric point, (c) the spin-wave expansion of higher-order exchange terms, (d) details of the fitting algorithm to optimize the magnetic exchange couplings, (e) further comparisons between calculated and measured magnetic excitations, (f) a discussion of the proximity of our best-fit model for $Na_2Co_2TeO_6$ to the Kitaev quantum spin liquid, and (g) the demonstration of metamagnetic transitions between triple-**q** and canted zigzag states in external fields.

[46] J. Wang and Z.-X. Liu, Effect of ring-exchange interactions in the extended Kitaev honeycomb model, Phys. Rev. B **108**, 014437 (2023).

[47] Y. Sizyuk, P. Wölfle, and N. B. Perkins, Selection of direction of the ordered moments in Na_2IrO_3 and α-$RuCl_3$, Phys. Rev. B **94**, 085109 (2016).

[48] J. G. Rau, P. A. McClarty, and R. Moessner, Pseudo-Goldstone Gaps and Order-by-Quantum Disorder in Frustrated Magnets, Phys. Rev. Lett. **121**, 237201 (2018).

[49] K. W. Plumb, J. R. Morey, J. A. Rodriguez-Rivera, H. Wu, A. A. Podlesnyak, T. M. McQueen, and C. L. Broholm, Antiferromagnetic and Orbital Ordering on a Diamond Lattice Near Quantum Criticality, Phys. Rev. X **6**, 041055 (2016).

[50] S. M. Winter, Y. Li, H. O. Jeschke, and R. Valentí, Challenges in design of Kitaev materials: Magnetic interactions from competing energy scales, Phys. Rev. B **93**, 214431 (2016).

[51] S. M. Winter, K. Riedl, P. A. Maksimov, A. L. Chernyshev, A. Honecker, and R. Valentí, Breakdown of magnons in a strongly spin-orbital coupled magnet, Nat. Commun. **8**, 1152 (2017).

[52] J. S. Gordon, A. Catuneanu, E. S. Sørensen, and H.-Y. Kee, Theory of the field-revealed Kitaev spin liquid, Nat. Commun. **10**, 2470 (2019).

[53] H. Godfrin and D. D. Osheroff, Multiple-spin-exchange calculation of the $T = 0$ properties of solid ^{3}He, Phys. Rev. B **38**, 4492 (1988).

[54] J. Nasu, J. Knolle, D. L. Kovrizhin, Y. Motome, and R. Moessner, Fermionic response from fractionalization in an insulating two-dimensional magnet, Nat. Phys. **12**, 912 (2016).

[55] A. Banerjee, C. A. Bridges, J.-Q. Yan, A. A. Aczel, L. Li, M. B. Stone, G. E. Granroth, M. D. Lumsden, Y. Yiu, J. Knolle, S. Bhattacharjee, D. L. Kovrizhin, R. Moessner, D. A. Tennant, D. G. Mandrus, and S. E. Nagler, Proximate Kitaev quantum spin liquid behaviour in a honeycomb magnet, Nat. Mater. **15**, 733 (2016).

[56] A. Banerjee, J. Yan, J. Knolle, C. A. Bridges, M. B. Stone, M. D. Lumsden, D. G. Mandrus, D. A. Tennant, R. Moessner, and S. E. Nagler, Neutron scattering in the proximate quantum spin liquid α-$RuCl_3$, Science **356**, 1055 (2017).

[57] S.-H. Do, S.-Y. Park, J. Yoshitake, J. Nasu, Y. Motome, Y. S. Kwon, D. T. Adroja, D. J. Voneshen, K. Kim, T.-H. Jang, J. H. Park, K.-Y. Choi, and S. Ji, Majorana fermions in the Kitaev quantum spin system α-$RuCl_3$, Nat. Phys. **13**, 1079 (2017).

[58] L. Janssen, E. C. Andrade, and M. Vojta, Magnetization processes of zigzag states on the honeycomb lattice: Identifying spin models for α-$RuCl_3$ and Na_2IrO_3, Phys. Rev. B **96**, 064430 (2017).

[59] C. Balz, L. Janssen, P. Lampen-Kelley, A. Banerjee, Y. H. Liu, J.-Q. Yan, D. G. Mandrus, M. Vojta, and S. E. Nagler, Field-induced intermediate ordered phase and anisotropic interlayer interactions in α-$RuCl_3$, Phys. Rev. B **103**, 174417 (2021).

[60] X. Hong, M. Gillig, W. Yao, L. Janssen, V. Kocsis, S. Gass, Y. Li, A. U. B. Wolter, B. Büchner, and C. Hess, Phonon thermal transport shaped by strong spin-phonon scattering in a Kitaev material $Na_2Co_2TeO_6$, arXiv:2306.16963.

[61] V. Kocsis and A. U. B. Wolter (private communication).

[62] R. D. Johnson, S. C. Williams, A. A. Haghighirad, J. Singleton, V. Zapf, P. Manuel, I. I. Mazin, Y. Li, H. O. Jeschke, R. Valentí, and R. Coldea, Monoclinic crystal structure of α-$RuCl_3$ and the zigzag antiferromagnetic ground state, Phys. Rev. B **92**, 235119 (2015).

[63] J. A. Sears, M. Songvilay, K. W. Plumb, J. P. Clancy, Y. Qiu, Y. Zhao, D. Parshall, and Y.-J. Kim, Magnetic order in α-$RuCl_3$: A honeycomb-lattice quantum magnet with strong spin-orbit coupling, Phys. Rev. B **91**, 144420 (2015).

[64] J. A. Sears, Y. Zhao, Z. Xu, J. W. Lynn, and Y.-J. Kim, Phase diagram of $\alpha - RuCl_3$ in an in-plane magnetic field, Phys. Rev. B **95**, 180411(R) (2017).

[65] J. A. Sears, L. E. Chern, S. Kim, P. J. Bereciartua, S. Francoual, Y. B. Kim, and Y.-J. Kim, Ferromagnetic Kitaev interaction and the origin of large magnetic anisotropy in α-$RuCl_3$, Nat. Phys. **16**, 837 (2020).

[66] A. Banerjee, P. Lampen-Kelley, J. Knolle, C. Balz, A. A. Aczel, B. Winn, Y. Liu, D. Pajerowski, J. Yan, C. A. Bridges, A. T. Savici, B. C. Chakoumakos, M. D. Lumsden, D. A. Tennant, R. Moessner, D. G. Mandrus, and S. E. Nagler, Excitations in the field-induced quantum spin liquid state of α-$RuCl_3$, npj Quantum Mater. **3**, 8 (2018).

[67] A. U. B. Wolter, L. T. Corredor, L. Janssen, K. Nenkov, S. Schönecker, S.-H. Do, K.-Y. Choi, R. Albrecht, J. Hunger, T. Doert, M. Vojta, and B. Büchner, Field-induced quantum criticality in the Kitaev system α-$RuCl_3$, Phys. Rev. B **96**, 041405(R) (2017).

[68] P. Lampen-Kelley, L. Janssen, E. C. Andrade, S. Rachel, J. Q. Yan, C. Balz, D. G. Mandrus, S. E. Nagler, and M. Vojta, Field-induced intermediate phase in α-$RuCl_3$: Non-coplanar order, phase diagram, and proximate spin liquid, arXiv:1807.06192.

[69] S. Toth and B. Lake, Linear spin wave theory for single-Q incommensurate magnetic structures, J. Phys. Condens. Matter **27**, 166002 (2015).

[70] P. Weinberg and M. Bukov, QuSpin: A Python package for dynamics and exact diagonalisation of quantum many body systems. Part I: spin chains, SciPost Phys. **2**, 003 (2017).

[71] P. Weinberg and M. Bukov, QuSpin: A Python package for dynamics and exact diagonalisation of quantum many body systems. Part II: bosons, fermions and higher spins, SciPost Phys. **7**, 020 (2019).

[72] W. Yao, Y. Zhao, Y. Qiu, C. Balz, J. R. Stewart, J. W. Lynn, and Y. Li, Magnetic ground state of the Kitaev $Na_2Co_2TeO_6$ spin liquid candidate, Phys. Rev. Res. **5**, L022045 (2023).